Acta metall. Vol. 36, No. 12, pp. 3149–3162, 1988
Printed in Great Britain.

0001-6160/88 $3.00 + 0.00

PRECIPITATE SHAPE TRANSITIONS DURING COARSENING UNDER UNIAXIAL STRESS

W. C. JOHNSON, M. B. BERKENPAS and D. E. LAUGHLIN
Department of Metallurgical Engineering and Materials Science, Carnegie Mellon University, Pittsburgh, PA 15213–3890, U.S.A.

(*Received* 27 *October* 1987; *in revised form* 16 *March* 1988)

Abstract—Precipitate shape transitions of elastically misfitting inclusions in the presence of a uniaxial stress field are examined for cubic materials using simple bifurcation theory. Both size-induced shape transitions that occur during growth of the precipitate under zero or constant stress and stress-induced shape transitions resulting from changes in the external stress field at constant precipitate volume and misfit are identified. Using elastic fields valid for small differences in elastic constants between precipitate and matrix, a dimensionless stress parameter and precipitate volume are identified from a Landau-type expansion that indicate the type and nature of permissible shape transitions. These dimensionless parameters incorporate the interfacial energy density, difference in elastic constants between precipitate and matrix, precipitate misfit, precipitate volume and external stress field into simple algebraic relationships. They indicate under what combination of material parameters a shape transition might be expected and whether the transition is continuous or discontinuous. Results of the model are applied using material parameters from a nickel-based alloy.

Résumé—A l'aide d'une théorie simple de bifurcation, nous étudions les transitions de forme des précipités pour des inclusions à désaccord élastique, en présence d'un champ de contraintes uniaxiales, dans le cas des matériaux cubiques. Nous identifions les deux types suivants de transitions de forme: transitions par effet de taille, qui apparaissent pendant la croissance du précipité sous contrainte nulle ou constante; transitions par effet de contraintes, qui résultent des variations du champ des contraintes externes pour des volumes de précipités et des désaccords identiques. En utilisant des champs élastiques valables pour de petites différences de constantes élastiques entre le précipité et la matrice, nous identifions un paramètre de contrainte sans dimension et un volume de précipité à partir d'un développement de type Landau, qui indique le type et la nature des transitions de forme permises. Ces paramètres sans dimension relient la densité d'énergie interfaciale, la différence de constantes élastiques entre le précipité et la matrice, le désaccord du précipité, le volume du précipité et le champ des contraintes externes à l'aide de simples relations algébriques. Ils indiquent pour quelle combinaison de paramètres d'un matériau donné on peut s'attendre à une transition de forme, et si cette transition est continue ou discontinue. Nous expliquons les résultats de ce modèle en utilisant les paramètres d'un alliage à base de nickel.

Zusammenfassung—Die Änderungen der Form von elastisch fehlpassenden Einschlüssen unter der Einwirkung eines einachsigen Spannungsfeldes werden für kubische Materialien mittels einer einfachen Bifurkationstheorie untersucht. Es werden zwei Formänderungen aufgezeigt, eine größeninduzierte, die während des Einschlußwachstums unter keiner oder konstanter Spannung auftritt, und eine spannungsinduzierte, die aus den Änderungen im äußeren Spannungsfeld, Einschlußvolumen und -fehlpassung konstant, folgt. Mittels elastischer Felder, die für kleine Unterschiede in den elastischen Konstanten von Einschluß und Matrix gelten, werden ein dimensionsloser Spannungsparameter und ein dimensionsloses Einschlußvolumen aus einer Entwicklung vom Landau-Typ gewonnen; diese Parameter geben Typ und Natur der erlaubten Formänderungen an. Die dimensionslosen Parameter fassen die Grenzflächenenergiedichte, den Unterschied der elastischen Konstanten zwischen Einschluß und Matrix, Fehlpassung des Einschlusses, Einschlußvolumen und äußeres Spannungsfeld in einfache algebraische Beziehungen. Sie beschreiben, unter welchen Kombinationen der Materialparameter eine Formänderung erwartet werden kann und ob diese Formänderung kontinuierlich oder diskontinuierlich abläuft. Ergebnisse des Modelles werden auf die Parameter einer Legierung auf Nickelbasis angewendet.

1. INTRODUCTION

Precipitate shape transitions during growth and coarsening are known to occur in many alloy systems. For example, in the nickel-based alloys, shape transitions from spheres to cubes, cubes to plates, and even the splitting of cubes into two or more plates are documented [1–3]. These shape transitions are often a result of changes in the relative contributions of the interfacial and elastic energies to the total system energy with increasing size of the precipitate. If the shape that minimizes the interfacial energy is different from that which minimizes the elastic energy, shape transitions during growth of the precipitate may be observed. Shape transitions may be first or second order in nature and have been examined by a number of authors [4–7].

Precipitate shape transitions and morphology changes also result from the application of an exter-

nal stress field (stress coarsening). These shape transitions include the sphere to ellipsoid transition in which the axis of revolution is either aligned in the direction of, or is perpendicular to, the external stress field and the corresponding cube to plate transition [8–12]. These are referred to as stress-induced shape transitions and are also a consequence of changes in the relative contributions of the elastic and interfacial energies to the total system energy. Several system-specific numerical calculations have been performed [12, 13] indicating that stress-induced transitions may be continuous or discontinuous in nature depending upon the precipitate size, external stress field, precipitate misfit, and the difference in elastic constants between precipitate and matrix. However, these calculations do not provide simple analytic relationships between the system parameters that allow general predictions to be made concerning the stability of the microstructure because of the large number of materials parameters that must be specified.

In this paper, we use analytical methods to examine preciptate shape transitions that may be expected to occur in certain materials with cubic symmetry. We identify shape transitions that may occur during the growth or coarsening of a precipitate in the presence of a constant external stress field as well as those shape transitions that result from changing the external stress at constant precipitate size. The approach employed is identical to that used previously to examine precipitate shape transitions in isotropic media [14]; energy-extremizing precipitate shapes of high symmetry and the changes in this symmetry due to external fields are considered. Two dimensionless parameters are identified that can be associated with the precipitate volume and external stress field, respectively, and which are used to identify some of the permissible shape transitions that may be observed in practice. Using this general model, examples are presented which use material constants from the $Ni–Ni_3Al$ system.

2. FORMULATION

2.1. Physical assumptions and symmetry principles

We consider a two phase elastic system in which the precipitate is embedded coherently in an infinite matrix. The elastic constants of the precipitate and matrix may be different but are restricted to exhibit either isotropic or cubic point group symmetries. The interfacial energy is eventually assumed to be isotropic, i.e. the effect of anisotropic interfacial energy is neglected. The crystallographic axes of the two phases are coincident. Transformation strains in the form of a dilatational misfit may be present due to differences in the lattice parameters of the two phases. Externally applied stress fields are limited to being uniaxial and directed along the [001] direction as depicted in Fig. 1.

To identify permissible transitions, we first determine the minimum symmetry of the variant morphology, both in the absence and presence of an applied stress field, and the minimum symmetry of the Wulff constructon for the interfacial energy (neglecting elastic effects). These symmetries suggest the possible orientations and shapes which the precipitate may exhibit. The elastic energy of the precipitate can break the symmetry of the precipitate shape [6, 14], leading to precipitate shapes of lower symmetry than predicted from group theory or the Wulff construction [15]. To identify which material parameters may effect elastically-induced shape transitions to shapes of lower symmetry, we then expand the elastic and interfacial energies of the system in terms of a shape (order) parameter about a shape which satisfies the Wulff construction symmetry. We then search for other energy-extremizing shapes among this set of allowable shapes. This approach allows analytical relationships between the material parameters and the applied stress to be obtained indicating the possible shape evolution and orientation during growth and coarsening of the precipitate.

The minimum symmetry of the variant morphology and of the Wulff shape is obtained from the intersection of the point groups of the precipitate and matrix and Curie group of the external field [16–19]. For two cubic phases in the absence of an external stress field, the minimum symmetry is simply

$$\frac{4}{m}\bar{3}\frac{2}{m} \cap \frac{4}{m}\bar{3}\frac{2}{m} = \frac{4}{m}\bar{3}\frac{2}{m} \tag{1}$$

This symmetry is lowered when an external field is applied along a four-fold axis of the system

$$\frac{4}{m}\bar{3}\frac{2}{m} \cap \frac{4}{m}\bar{3}\frac{2}{m} \cap \frac{\infty}{m}\frac{2}{m}\frac{2}{m} = \frac{4}{m}mm. \tag{2}$$

Higher symmetries than indicated by equations (1) or (2) are always allowed [16]. Since one symmetry can be represented by many shapes, there are a number of precipitate shapes that a coherent (unstressed) cubic precipitate in a cubic matrix can possess [18].

When elastic stresses are present in the system, the symmetry of the equilibrium precipitate shape may be less than that of the Wulff shape or variant morphology [15]. However, we would expect the shapes of small precipitates to possess the minimum symmetry given by Curie's principle (i.e. that of the Wulff construction), when the interfacial energy dominants the elastic energy. As the size of the precipitate increases, elastic effects become more important and elastically-induced shape transitions become possible.

In order to obtain information on the relative importance of the material parameters in determining precipitate shape, we limit our analysis to ellipsoidal precipitate shapes. This limitation is imposed for several reasons. First, the sphere is a highly symmetric shape that is often observed experimentally in the nickel-based alloys [8, 20, 21], especially when the particles are small. Second, shape transitions from spheres to ellipsoids are observed in the presence of

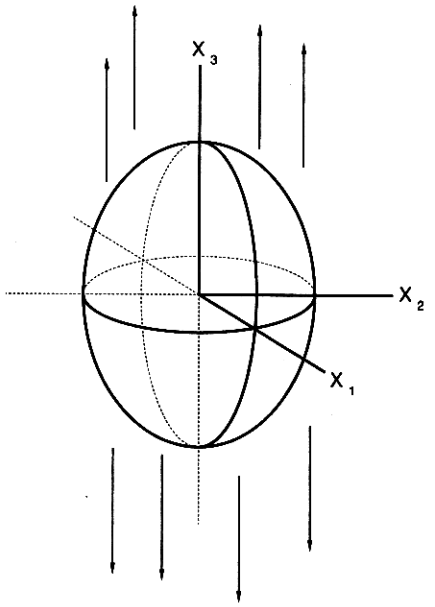

Fig. 1. Schematic diagram of an ellipsoidal precipitate in an infinite matrix. The semi-axes a_1, a_2 and a_3 are coincident with x_1, x_2 and x_3 coordinate directions respectively. The external stress is applied along the x_3 direction.

an external stress field [8]. Third, the elastic energy of ellipsoids can be determined more simply than other precipitate shapes and, finally, the elastic energy of inhomogeneous rectangular parallelepipeds in isotropic media (which are also observed experimentally in these systems) show the same functional behavior with respect to shape as do ellipsoids [22, 23]. Of course, spheres and cubes are both permissible shapes obtained from Curie's principle.

The elastic and interfacial energies depend on the dimensions of the ellipsoid as well as the material parameters. The precipitate shape can be completely characterized in terms of the lengths of ellipsoid semiaxes, a_1, a_2 and a_3. However, in order to make appropriate use of the system symmetry, the precipitate shape is defined in terms of the following three parameters [6].

$$S = (2a_3 - a_1 - a_2)/(a_1 + a_2 + a_3) \tag{3}$$

$$T = (a_1 - a_2)/(a_1 + a_2 + a_3) \tag{4}$$

$$V = \frac{4\pi}{3} a_1 a_2 a_3 \tag{5}$$

where V is the volume of the precipitate and S and T are dimensionless shape parameters. When the precipitate is spherical, $S = T = 0$. When it is an ellipsoid of revolution (spheroid), $T = 0$. S varies from -1 to 2 and may be thought of as an aspect ratio: when $T = 0$, $S = -1$ corresponds to a disk while $S = 2$ corresponds to a needle. In both cases the axis of revolution coincides with the x_3 axis.

2.2. Energy extrema

We now search for energy-extremizing precipitate shapes in the absence and presence of the external field. We do so by expanding the energy of the system into a Taylor series about the highly symmetric state, $S = T = 0$, and then searching for neighboring less symmetric states that are also energy extrema. This approach is identical to a Landau expansion where the shape parameter is the internal variable. In what follows, it is assumed that $T = 0$ to simplify the analysis.†

The total energy of the system, E^t, is

$$E^t(S, V) = E^s + E^e \tag{6}$$

where E^s and E^e are the interfacial and elastic energies, respectively. It is convenient to scale the total energy by the interfacial energy of a sphere giving

$$\Phi = \frac{E^t}{4\pi\sigma}\left(\frac{4\pi}{3V}\right)^{2/3} \tag{7}$$

where σ is the interfacial energy density.

Expanding Φ in terms of the shape parameter, S, about $S = 0$ gives

$$\Phi = \sum_{n=0}^{\infty} \frac{1}{n!} \Phi_n S^n \tag{8}$$

where

$$\Phi_n = \left(\frac{\partial^n \Phi}{\partial S^n}\right)_{S=0}. \tag{9}$$

The energy-extremizing solutions must satisfy

$$\left(\frac{\partial \Phi}{\partial S}\right)_V = 0 \tag{10}$$

or, from equation (8)

$$0 = \Phi_1 + \Phi_2 S + \tfrac{1}{2}\Phi_3 S^2 + \tfrac{1}{6}\Phi_4 S^3 + \cdots \tag{11}$$

The Taylor coefficients, Φ_n, are functions of the precipitate volume and the material parameters. They can also be expressed in terms of the corresponding Taylor coefficients of the interfacial and elastic energies as

$$\Phi_n = E_n^s + \frac{E_n^e}{4\pi\sigma}\left(\frac{4\pi}{3V}\right)^{2/3} \tag{12}$$

where

$$E^s = 4\pi\sigma\left(\frac{3V}{4\pi}\right)^{2/3} \sum_{n=0}^{\infty} \frac{1}{n!} E_n^s S^n \tag{13}$$

and

$$E^e = \sum_{n=0}^{\infty} \frac{1}{n!} E_n^e S^n \tag{14}$$

The Taylor coefficients for the interfacial energy are numerical constants when the interfacial energy density is independent of orientation [6].

†Inclusion of $T \neq 0$ expands the model to include the other two variants with major or minor axes directed along the x_1 or x_2 axes.

The coefficients for the elastic energy depend upon the dilatational transformation strain (ϵ), the applied stress (σ^A), and the elastic constants of both the precipitate (C_{ij}^P) and matrix (C_{ij}) phases. For isotropic elasticity, the Taylor coefficients may be obtained in analytical form [6] while for cubic anisotropy they must be computed numerically. Since numerical computation precludes the ability to obtain analytical relationships between all the material parameters, the Taylor coefficients are approximated to first order in the difference in elastic constants between precipitate and matrix. The Taylor coefficients for the elastic energy then assume the form

$$E_n^e = \frac{V\epsilon^2(C_{11}+2C_{12})L_n}{2} + \frac{V\epsilon\tau(C_{11}+2C_{12})^2K_n}{(C_{11}+C_{12})} \tag{15}$$

$$L_n = -F_n(1+2(\Delta\bar{C}_{11}+2\Delta\bar{C}_{12})] + \Delta\bar{C}_{12}G_n + (\Delta\bar{C}_{11}-\Delta\bar{C}_{12})H_n \tag{16}$$

$$K_n = (\bar{C}_{11}\Delta\bar{C}_{12}-\bar{C}_{12}\Delta\bar{C}_{11})F_n + (\Delta\bar{C}_{11}-\Delta\bar{C}_{12})I_n \tag{17}$$

$$\Delta\bar{C}_{ij} = (C_{ij}^P - C_{ij})/(C_{11}+2C_{12}) \tag{18}$$

$$\tau = \frac{\sigma^A(C_{11}+C_{12})}{(C_{11}-C_{12})(C_{11}+2C_{12})} \tag{19}$$

based on the assumption that

$$|\Delta\bar{C}_{ij}| \ll 1. \tag{20}$$

The quantities, F_n, G_n, H_n and I_n depend only on the elastic constants of the matrix, are evaluated for a sphere ($S=0$), and can be solved using a numerical quadrature integration scheme. These quantities are given in the Appendix.

3. RESULTS

3.1. Shape transitions in the absence of applied stress

In the absence of an applied stress field, $\tau = 0$ and E_n^e depends only upon L_n. It then follows from group theory or direct computation that $L_1 = 0$, since $F_1 = G_1 = H_1 = 0$. The coefficients for the system energy then become.

$$\Phi_0 = 1 + \frac{E_0^e}{4\pi\sigma}\left(\frac{4\pi}{3V}\right)^{2/3} \tag{21}$$

$$\Phi_1 = 0 \tag{22}$$

and, for $n > 1$

$$\Phi_n = E_n^s + \frac{L_n}{4\pi\sigma}\left(\frac{4\pi}{3V}\right)^{2/3}. \tag{23}$$

Substituting equations (21)–(23) into equation (11) gives

$$0 = S\left[E_2^s(1-\Lambda) + \frac{(E_3^sL_2 - L_3E_2^s\Lambda)S}{2L_2} + \frac{(E_4^sL_2 - L_4E_2^s\Lambda)S^2}{6L_2} + \cdots\right] \tag{24}$$

where we have introduced the dimensionless precipitate size, Λ

$$\Lambda = \frac{-\epsilon^2V(C_{11}+2C_{12})}{8\pi\sigma E_2^s}\left(\frac{4\pi}{3V}\right)^{2/3}L_2. \tag{25}$$

The roots of equation (24) are those precipitate shapes that extremize the system energy for a given precipitate size Λ. For precipitate shape transitions to occur, there must exist more than one extremizing shape for a given precipitate volume, and the relative stability of these shapes must change as the precipitate volume changes. The different types of transitions that may occur therefore, depend on the relative signs and magnitudes of the coefficients of the energy expansion which, in turn, are functions of the materials parameters and precipitate volume.

The nature and conditions for an elastically induced shape transition can be identified by searching for shape transitions in the vicinity of $S=0$. If $\Phi_4 > 0$, it is necessary to retain only the first few terms in the energy expansion of equation (8). Dropping terms of S^5 and higher in the energy expansion, the roots of equation (24) in terms of Φ_n are

$$S = 0, \quad \frac{3\Phi_3}{2\Phi_4}\left[-1 \pm \left(1 - \frac{8\Phi_2\Phi_4}{3\Phi_3^2}\right)^{1/2}\right]. \tag{26}$$

Higher order terms must be retained to determine additional roots, find roots when $\Phi_4 \leqslant 0$, or correct for roots far from $S=0$.

The first root of equation (26), $S=0$, is independent of precipitate size. The two additional roots intersect the first at $\Lambda = 1$ corresponding to $\Phi_2(\Lambda = 1) = 0$. Such an intersection point is termed a bifurcation point and entails a change in stability of the equilibrium solution [24]; a solution that is a minimum in the energy must become a maximum. Here, since the sphere is an energy minimizing shape for small Λ, the sphere loses stability at $\Lambda = 1$ and a transition from sphere to spheroid occurs as the precipitate size increases.

The shape transition from sphere to spheroid occurs continuously when $\Phi_3(\Lambda = 1) = 0$ and discontinuously otherwise. When $\Phi_3(\Lambda = 1) \neq 0$, stable equilibrium solutions for shapes other than a sphere exist for $\Lambda < 1$. The value of Λ at which the two new extremizing solutions first appear, Λ_t, is known as a turning point and is determined by setting the quantity under the radical sign in equation (26) to zero, i.e. when

$$8\Phi_2\Phi_4 = 3\Phi_3^2. \tag{27}$$

The global energy minimum must change discontinuously from a sphere to an oblate or prolate spheroid [6] at a value of Λ given by $\Lambda_t < \Lambda < 1$. The precise value of Λ is given by solution to the equation

$$\Phi_3^2 - 4\Phi_2\Phi_4 = 0. \tag{28}$$

The transition is from $S = 0$ to

$$S = -(1 + \sqrt{3}/3)\Phi_3/\Phi_4. \tag{29}$$

The transition is from sphere to oblate spheroid when $\Phi_3/\Phi_4 > 0$ and to prolate spheroid otherwise. Consequently, if the precipitate is kineticly able to assume the shape that provides the global energy minimum and $\Phi_3/\Phi_4 \neq 0$, the shape will change discontinuously during growth from a sphere to a spheroid prior to obtaining a critical volume, V_c. For the size-induced shape transition in the absence of an applied stress, this jump usually occurs very close to $\Lambda = 1$.

The critical size, V_c, at which the sphere loses stability occurs when $\Lambda = 1$ and is given by

$$V_c^{1/3} = \frac{-8\pi\sigma E_2^s}{\epsilon^2(C_{11} + 2C_{12})L_2}\left(\frac{3}{4\pi}\right)^{2/3} \tag{30}$$

V_c is positive only when $L_2 < 0$, since $E_s^2 > 0$.

When the system is elastically isotropic, the Taylor coefficients can be obtained analytically. The values for these coefficients are: $F_2 = G_2 = 0$ and $H_2 = 12(1 + v)^2/25(1 - v)^2$. When the system is isotropic and inhomogeneous, the critical volume for the shape bifurcation becomes

$$V_c^{1/3} = \frac{-25\pi\sigma(1 - v)^2 E_2^s}{3\epsilon^2(C_{44}^P - C_{44})(1 + v)^2}\left(\frac{3}{4\pi}\right)^{2/3}. \tag{31}$$

V_c is physical only when $C_{44}^P < C_{44}$; the shear modulus of the precipitate is less than that of the matrix. When the precipitate is elasically harder than the matrix, $C_{44}^P > C_{44}$, the sphere is the only equilibrium shape. Equation (31) is equivalent to previous results [6] if the energy is expressed to first order in the difference in elastic constants. When the system is elastically isotropic and homogeneous, $L_2 = 0$, and there is no bifurcation point. The only equilibrium solution is the sphere which is stable for all precipitate sizes.

The fine lines in Fig. 2 display the energy-extremizing precipitate shapes in the absence of an external stress field as a function of the dimensionless precipitate size, Λ, for an isotropic matrix with elastic constants corresponding to those of nickel, $C_{12} = 11.7 \times 10^4$ MPa, $C_{44} = 9.47 \times 10^4$ MPa and $C_{11} = C_{12} + 2C_{44}$. This is a bifurcation diagram exhibiting only equilibrium solutions. As in all subsequent figures, the solid lines denote energy minima (linearly stable) and the broken lines energy maxima (unstable): no distinctions being made between global and local (metastable) equilibrium states. Fine lines represent extrema in the absence of external stress and heavy lines extrema in the presence of an external stress. The extrema in all figures are calculated exactly, the Landau-type expansion only being used to indicate the nature of the shape transition and the critical size of the precipitate. In the isotropic case $\Phi_4 > 0$, except for very soft precipitates, and $\Phi_3 > 0$. For very small precipitate sizes, $\Lambda \ll 1$, the sphere ($S = 0$) is the only extremum and it is stable. When Λ is slightly less than 1, there are two stable solutions separated by an unstable solution. One stable solution is a sphere and the other is an oblate spheroid ($S < 0$). When $\Lambda = 1$, two extremizing solutions intersect and the sphere becomes unstable, i.e. an energy maximum. There are two stable solutions for $\Lambda > 1$: one is an oblate spheroid ($S < 0$) and the other a prolate spheroid ($S > 0$).

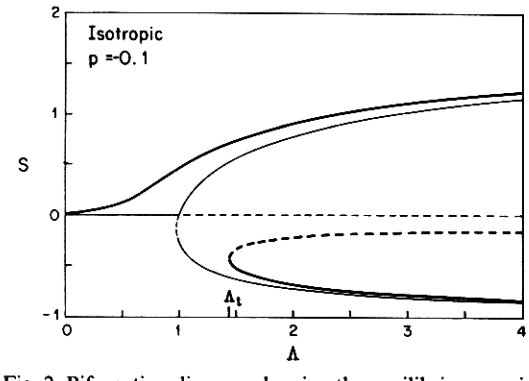

Fig. 2. Bifurcation diagram showing the equilibrium precipitate shapes in the presence (heavy lines) and absence (fine lines) of an external stress field as a function of the precipitate size, Λ, for a dimensionless stress parameter of value $p = -0.1$. The system is elastically isotropic with the shear modulus of the precipitate less than that of the matrix. The solid lines represent energy minima and the broken lines energy maxima.

When the precipitate and matrix possess the same cubic elastic constants, the sign of L_2 is determined by the sign of F_2. $F_2 < 0$ when the Zener aspect ratio, $A = 2C_{44}/(C_{11} - C_{12}) > 1$. Thus there exists a critical precipitate volume given by equation (30) where two solutions intersect and the sphere loses stability. Differences in the elastic constants between precipitate and matrix may change the value of L_2 and hence the volume where the sphere loses stability.

When $A < 1$, $L_2 > 0$, and there is no bifurcation from the solution $S = 0$. Although other solutions may still exist, the solutions do not intersect. These solutions are known as isolated solutions. For systems in which $A < 1$, the elastically soft crystallographic directions are $\langle 111 \rangle$ and ellipsoids of revolution may be expected to have their axis of revolution along this direction [25]. Thus the solutions obtained from this treatment in which the axis of revolution is constrained to lie along $\langle 100 \rangle$, may not be that solution observed experimentally. Analyzing this bifurcation requires a much more extensive treatment incorporating orientational effects and additional order parameters. Further analyses presented here will assume that $A > 1$ unless otherwise stated.

The thin lines of Fig. 3 show the energy-extremizing precipitate shapes in the absence of an external stress field as a function of the dimensionless precipitate size, Λ, for a Ni(Al) matrix ($C_{11} = 11.24 \times 10^4$ MPa, $C_{12} = 6.27 \times 10^4$ MPa, $C_{44} = 5.69 \times 10^4$ MPa) and Ni_3Al precipitate ($C_{11} = 16.66 \times 10^4$, $C_{12} = 10.65 \times 10^4$, $C_{44} = 9.92 \times 10^4$) [12]. These elastic constants are extrapolated from room temperature up to 750°C [12]. For this set of elastic constants, $A = 2.29$. The transition of the stable precipitate

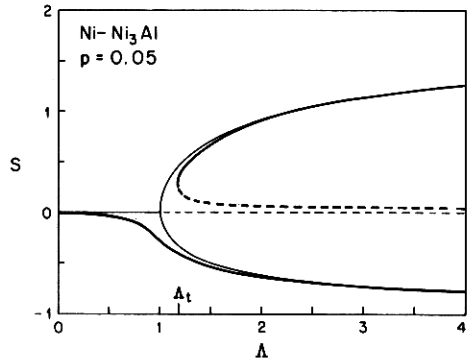

Fig. 3. Bifurcation diagram depicting the equilibrium shapes of Ni_3Al precipitates in a Ni matrix as a function of the dimensionless precipitate size, Λ, at 750°C. Solid lines represent energy minima and broken lines energy maxima. The fine lines denote equilibrium shapes in the asbsence of an applied stress while the heavy lines the equilibrium shapes in the presence of a dimensionless stress, $p = 0.05$.

shape from sphere to ellipsoid appears to be almost a continuous transition. However, since the coefficient $\Phi_3(\Lambda = 1) \neq 0$, the transition is first order, albeit a very weak one. In this case, the precipitate shape that is a global energy minimum jumps discontinuously from a sphere to a prolate spheroid ($S = 0.04$) at a value of Λ just slightly less than one, as given by solution of equation (28).

In constructing Fig. 3, specific elastic constants are assumed for both the precipitate and matrix phases. Changing the elastic constants of the precipitate can alter the shape of the equilibrium solution and change the nature of the transition. Since the shape transition is weakly discontinuous, a small change in the precipitate elastic constants can give rise to a continuous transformation when $\Phi_3(\Lambda = 1) = 0$. Other combinations of precipitate elastic constants allow the jump transition to proceed discontinuously, from sphere to oblate ellipsoid, similar to the behavior displayed by the isotropic system. In most of the cubic alloy systems examined, the transition is more weakly first order than for the isotropic case.

3.2. Shape transitions under applied stress

In the presence of a uniaxial stress directed along the cube axis x_3, the Taylor coefficients to the system energy become

$$\Phi_1 = p\Lambda \tag{32}$$

$$\Phi_2 = E_2^s(1 - \Lambda) + \frac{K_2}{K_1}p\Lambda \tag{33}$$

$$\Phi_n = E_n^s - \frac{E_2^s L_n}{L_2} + \frac{K_n}{K_1}p\Lambda \tag{34}$$

where the various coefficients are given in the Appendix. For an isotropic system, $F_2 = G_2 = 0$, $H_2 = 12(1+v)^2/25(1-v)^2$, $I_1 = -2(1+v)/5(1-v)$ and the parameter p simplifies to

$$p = \frac{5\tau E_2^s(1-v)}{3\epsilon} \tag{36}$$

In the isotropic limit, p is independent of the difference in elastic constants between precipitate and matrix.

If terms in the energy expansion of order S^5 and higher are once again neglected, the equilibrium precipitate shapes are given by the roots of the cubic polynomial

$$\Phi_1 + \Phi_2 S + \tfrac{1}{2}\Phi_3 S^2 + \tfrac{1}{6}\Phi_4 S^3 = 0. \tag{37}$$

For equation (37) one or three real roots exist; the number being determined by the sign of the determinant $D(\Lambda)$

$$D(\Lambda) = (8\Phi_2\Phi_4 - 3\Phi_3^2)(\Phi_2^2 - 2\Phi_1\Phi_3) - 2\Phi_1\Phi_2\Phi_3\Phi_4 + 9\Phi_1^2\Phi_4^2. \tag{38}$$

It is immediately evident that the sphere, $S = 0$, is no longer a solution as the coefficient Φ_1 now assumes a value different from zero. Since $D(\Lambda)$ changes with precipitate size, the number of equilibrium precipitate shapes may also change with the precipitate size. When $D(\Lambda) < 0$, there are three real roots to equation (38) and hence three equilibrium precipitate shapes. There is only one equilibrium shape when $D(\Lambda) > 0$. When $D(\Lambda) = 0$, there are three real roots; at least two of the roots are equal and correspond to a turning point. When $\Lambda \ll 1$, the precipitate is small and only one equilibrium shape is obtained. Whether the shape is an oblate or prolate spheroid at small Λ depends upon the sign of Φ_1. If $\Phi_1 < 0$, then $S > 0$ and the equilibrium shape is a prolate spheroid for small Λ. Likewise, $S < 0$ for $\Phi_1 > 0$. Thus it is the sign of Φ_1 that determines the direction in which the energy and, hence, equilibrium precipitate shape is perturbed by the applied stress field [14].

The sign of Φ_1 is determined by the signs of both p and Λ in equation (32). The signs of ρ and Λ depend upon the material parameters and the applied stress. If we continue to limit ourselves to systems in which the Zener aspect ratio is greater than one, then $\Lambda > 0$ and the sign of Φ_1 is equal to the sign of p. Since $I_1 < 0$, the sign of p is equal to the sign of $\tau(\Delta C_{11} - \Delta C_{12})/\epsilon$. In principle, the sign of L_2 may change because of the difference in elastic constants between precipitate and matrix. For a number of cubic alloy systems examined, this appears to be true only when the anisotropy ratio is close to one and the difference in elastic constants between phases is large.

$$p = \frac{2\tau(C_{11} + 2C_{12})(\Delta\bar{C}_{11} - \Delta\bar{C}_{12})I_1 E_2^s}{\epsilon(C_{11} + C_{12})[F_2 + \Delta\bar{C}_{11}(2F_2 - H_2) + \Delta\bar{C}_{12}(4F_2 - G_2 + H_2)]} \tag{35}$$

For an isotropic system, $\Lambda > 0$ when $C_{44}^p - C_{44} < 0$ and the sign of Φ_1 is again determined by p. The sign

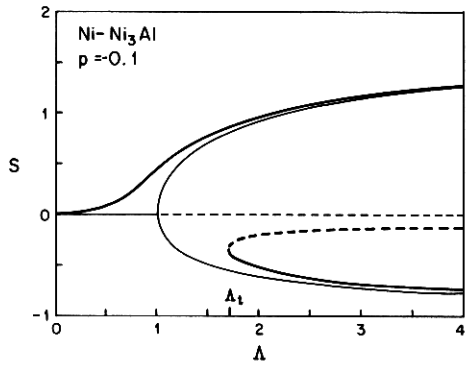

Fig. 4. Equilibrium shapes of Ni_3Al precipitates in a Ni matrix in the presence of an applied stress, $p = -0.1$ (heavy lines). The bifurcation is broken in the direction opposite to that of Fig. 3. At large values of Λ, the global energy minimum changes from prolate to oblate spheroid for sufficiently large values of p.

of Φ_1 for the general isotropic case is thus the same as the sign of $\tau(C_{44} - C_{44}^P)/\epsilon$. Thus, for the isotropic system, it is the difference in shear moduli between precipitate and matrix that determines precipitate shape, while for the anisotropic case it is $\Delta C_{11} - \Delta C_{12}$.

The heavy lines in Fig. 2 show the equilibrium precipitate shapes in the presence of an external stress as a function of Λ for an isotropic system in which $C_{44}^P < C_{44}$. When $p \neq 0$, the applied stress breaks the bifurcation derived in the absence of stress and the solutions no longer intersect. When $p < 0$, the prolate spheroid is the equilibrium shape for small values of Λ. At $\Lambda = \Lambda_t$, determined by setting $D(\Lambda) = 0$ in equation (38), two new equilibrium solutions appear for $S < 0$. For small values of Λ, the prolate spheroid is the global energy minimum and remains so past the appearance of the new equilibrium solutions at Λ_t. However, for sufficiently large values of Λ, the prolate spheroid may become a local minimum and the oblate spheroid a global minimum. This means that if a growing precipitate is able to assume the shape of lowest energy, a shape transition from prolate to oblate spheroid may occur at some new critical size. Whether or not there is a discontinuous change in the global stability from prolate to oblate spheroid (or from oblate to prolate), depends upon the magnitude of the applied stress and the difference in elastic constants between precipitate and matrix phases.

The heavy lines in Figs 3 and 4 display the precipitate shapes that extremize the system energy in the presence of an applied stress for the Ni(Al)–Ni_3Al two-phase system. In Fig. 3, $p > 0$, $\Phi_1 > 0$ and the oblate spheroid is the stable equilibrium solution at small values of Λ. The oblate spheroid is the global energy minimum for all values of Λ although the prolate spheroid is a metastable shape for $\Lambda > \Lambda_t$. Consequently, no shape transitions would be expected under constant external stress during the growth of the precipitate. In Fig. 4, $p < 0$ and the prolate spheroid is the shape that is the global energy minimum for small values of Λ. At a sufficiently large value of Λ, however, the global energy minimum may switch from the prolate spheroid to the oblate spheroid. The change in global stability again depends upon the applied stress and the difference in elastic constants between precipitate and matrix and requires a detailed energy analysis to determine if it can occur.

Size-induced shape transitions corresponding to the bifurcation plots of Figs 2–4 are displayed schematically in Fig. 5 where the dimensionless energy is plotted as a function of precipitate shape for various sizes of the precipitate. Figure 5(a) depicts the case in the absence of applied stress, $p = 0$. For small dimensionless precipitate sizes, the sphere is the only stable solution while for larger sizes two minima exist with the sphere being an energy maximum. Figure 5(b) shows the case with $p > 0$. Even at small dimensionless precipitate sizes, the oblate spheroid is the global energy minimum. When $p < 0$, as illustrated in Fig. 5(c), the prolate spheroid is the lowest energy shape changing discontinuously to an oblate spheroid at large sizes. Changing the magnitude of p may stabilize the prolate spheroid with respect to that of the oblate spheroid. This behavior for the Ni–Al system is also shown in the numerical calculations of Miyazaki *et al.* [12]. A projection of all the loci of energy extrema in Fig. 5 plotted as a function of Λ results in bifurcation diagrams similar to those of Figs 2–4.

Thus far we have identified size-induced shape transitions that occur during the growth of the precipitate under constant external stress. It is also possible to induce shape transitions by changing the sign and/or magnitude of the applied stress [14, 26]. Stress-induced shape transitions are shown schematically in Fig. 6 where the dimensionless energy is plotted as a function of aspect ratio, S, for various values of the dimensionless stress parameter, p. Figure 6(a) displays the case where $\Lambda < 1$. The energy-minimizing shape can be seen to change continuously from an oblate to a prolate ellipsoid and back as the stress is cycled between positive and negative p. Figure 6(b) showes the energy dependence on shape at the bifurcation point for different values of external stress. For all three values of p, there is only one minimum; however, when $p = 0$, there is also an extremum at $S = 0$ which is a saddle point. Since Λ_t is a function of the applied stress, stress induced transitions near $\Lambda = 1$ are complicated and may be either discontinuous or continuous in nature. For $\Lambda > 1$, as shown in Fig. 6(c), stress-induced shape transitions are discontinuous jumping from an oblate spheroid to prolate spheroid as p decreases from positive to negative values. The sphere is never a stable equilibrium shape even when the external field is absent. The discontinuous jump in shape, as measured by the change in the equilibrium aspect ratio S, becomes greater as Λ increases.

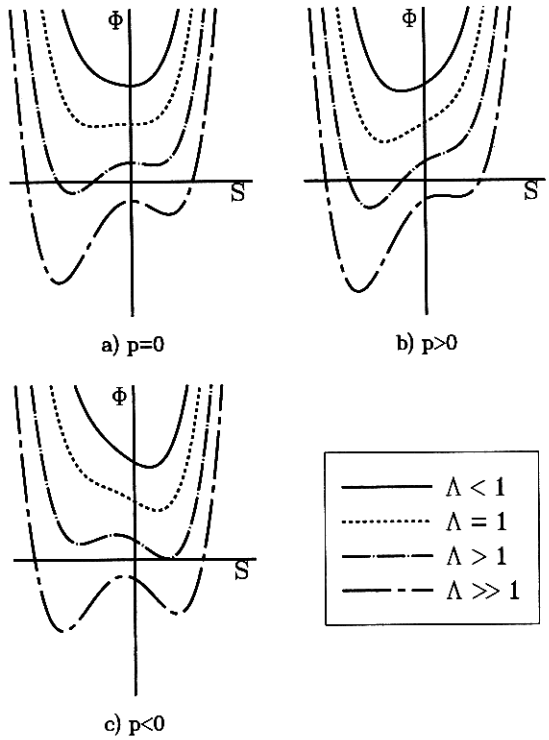

Fig. 5. A schematic representation of the dimensionless energy as a function of the shape parameter, S, for various dimensionless precipitate sizes Λ. (a) When $p = 0$, the sphere is always an equilibrium shape. Near $\Lambda = 1$, two new energy minima appear and the sphere becomes an energy maximum. In this example, the oblate spheroid remains the global energy minimum for large Λ. (b) When $p > 0$, the oblate spheroid is an energy minimum for all precipitate sizes although for larger Λ the prolate spheroid becomes metastable. (c) When $p < 0$, the prolate spheroid is a linearly stable equilibrium state for all precipitate sizes. For $\Lambda > 1$, the oblate spheroid becomes metastable and, for this example, becomes the global energy shape when Λ is sufficiently large.

Stress-induced shape transitions can also be succinctly displayed best on bifurcation diagrams. Figure 7 is such a diagram in which the equilibrium precipitate shapes that extremize the system energy are plotted as a function of the dimensionless stress parameter for various values of the dimensionless precipitate size. Once again, the solid lines represent stable equilibrium solutions and the broken lines unstable shapes. The heavy lines are used to represent the global equilibrium solutions while the fine solid lines correspond to the metastable precipitate shapes. For values of $\Lambda < 1$, equilibrium precipitate shapes change continuously with changes in the external field. When $\Lambda > 1$, discontinuous changes in the equilibrium shape are observed with changes in the external field. For this situation, there exist metastable precipitate shapes over certain ranges of the external stress separated by an activation barrier from the precipitate shape that gives the global energy minimum. The activation barrier disappears at that external stress where $dp/dS = 0$.

4. DISCUSSION

From the bifurcation analysis, two dimensionless parameters, Λ and p, have been identified that can be used to indicate the various types of shape transitions that may occur both in the absence and presence of an external stress field. Λ is a measure of the precipitate volume while p is a measure of the external stress field. The nature of the size-induced and stress-induced transitions can be understood entirely in terms of these two parameters.

In the absence of an applied stress, size-induced shape transitions are governed by the bifurcation parameter, Λ. The sign of Λ is determined by the difference in elastic constants between precipitate and matrix and the elastic anisotropy of the matrix. Λ is independent of the sign of ϵ. If the Zener anisotropy ratio of the matrix is less than one, then $\Lambda < 0$ (since $L_2 > 0$); the sphere remains a stable shape for all precipitate sizes. When $A > 1$, $\Lambda > 0$ and there exists a critical precipitate volume where the sphere loses stabilty with respect to an ellipsoid. For an isotropic matrix, $A = 1$, the sphere remains stable for all precipitate sizes when $C_{44}^{P} \geqslant C_{44}$. If $C_{44}^{P} < C_{44}$, a spherical precipitate will eventually become unstable.

The sphere loses stability at the bifurcation point corresponding to $\Lambda = 1$. At this point two equilibrium solutions intersect and a spherical precipitate becomes unstable with respect to changes in aspect ratio. The size-induced shape transition (following

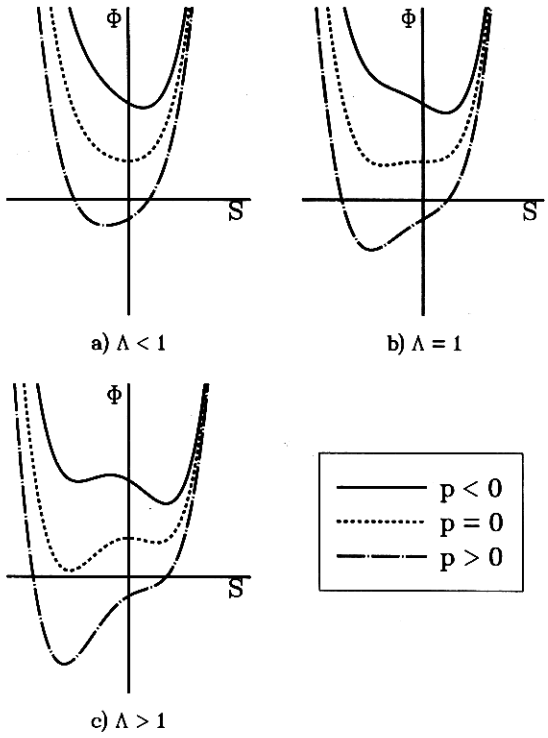

Fig. 6. Schematic illustration of the dimensionless energy changes associated with stress-induced shape transitions for various sized precipitates. (a) A continuous stress-induced shape transition in p is observed for small precipitate sizes, $\Lambda < 1$. (b) A weak discontinuous stress-induced shape transition in p usually occurs for a critical precipitate size, and (c) a large discontinuous stress-induced shape transition in p occurs for large precipitate sizes, $\Lambda \gg 1$.

the global energy minimum) from sphere to spheroid almost always occurs in the region $0.95 < \Lambda < 1$ and $\Lambda = 1$ is usually a very good approximation to the size at which the transition should be observed. Although a bifurcation point does not exist when the ellipsoidal axes are constrained to be coincident with the crystallographic axes for systems in which $A < 1$, shape transitions may still occur as the result of the existence of isolated solutions. These isolated solutions do not appear to exist for isotropic systems. Shape transitions may also occur when the axis of revolution is no longer constrained to lie along a cube axis.

In the early stages of precipitate growth only one equilibrium shape exists and this shape is an energy minimum. At larger precipitate sizes ($\Lambda > 1$), three equilibrium solutions may exist: two minima and one maximum. These solutions do not intersect for large Λ and, consequently, do not change stability. However, the gobal stability of the solution may change with increasing size leading to the possibility of a shape change from a metastable solution to the global solution. Such a shape change requires surmounting an activation barrier.

The critical precipitate size corresponding to $\Lambda = 1$ is given by equation (30) and indicates how the various materials parameters interact to stabilize the sphere. For example, the critical radius increases linearly with the interfacial energy density and is inversely proportional to the square of the misfit. Also, the greater the elastic anisotropy of a homogeneous system, the smaller the critical radius, as reflected through the parameter L_2.

Although the shape transitions have been determined for ellipsoidal precipitates, the qualitative and some quantitative aspects of the analysis are also expected to be applicable to cuboidal precipitates. The cuboids are permissible precipitate shapes from the symmetry analysis and the cuboidal shape can be quantified in terms of the same shape parameters as the ellipsoid, S, T, and V [23] where S and T are defined as in equations (3) and (4), with the semiaxes of the ellipsoid replaced by half the cuboid edge lengths. When $S = T = 0$, the precipitate shape is a cube while $T = 0$ corresponds to a rectangular parallelepiped with two of the three independent edge lengths being equal. Since the functional dependence of the elastic self energy of inhomogeneous cuboids with respect to aspect ratio, S, is very similar to that of ellipsoidal precipitates [22, 23], the qualitative observations for ellipsoids should be valid for cuboids as well.

As an example of shape transitions in the absence of stress, we again examine the Ni(Al)–Ni_3Al binary system. The Ni_3Al precipitates are usually observed to be cuboids which remain coherent up to large sizes as shown in the micrograph of Fig. 8, courtesy of M. J. Kaufman. The Ni–17at.%Al binary alloy was solution treated and then slow cooled to 1100°C where it was held for one hour, followed by a water quench. Two distinct precipitate shapes are observed, smaller cubes with edge length of approximately

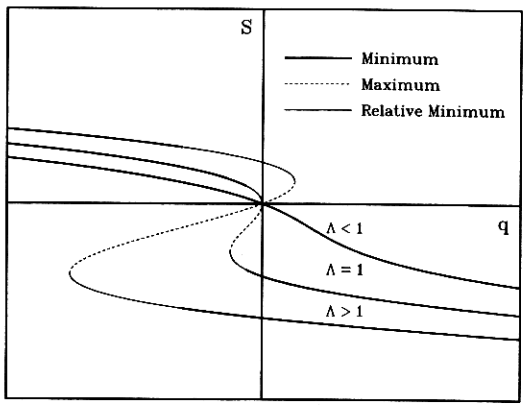

Fig. 7. A bifurcation diagram representing the precipitate shape that extremizes the system energy as a function of the dimensionless stress parameter for several dimensionless precipitate sizes. The heavy lines correspond to global minima, the fine lines local minima and the broken lines energy maxima. For small precipitate sizes the shape transitions are continuous and become discontinuous as the size of the precipitate increases. For the larger precipitates, two linearly stable precipitate shapes may be observed separated by a significant activation energy.

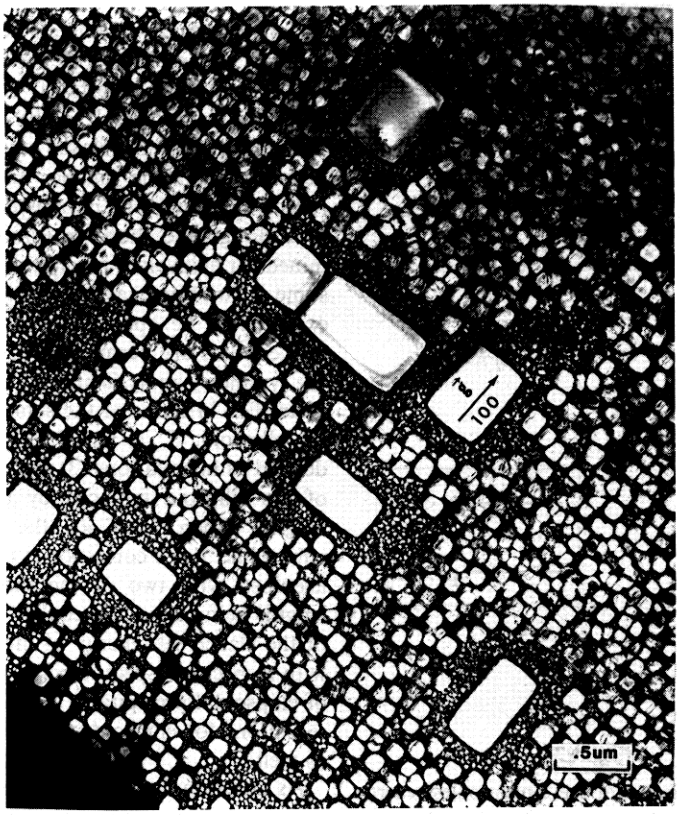

Fig. 8. Centered dark field micrograph using [100] reflections, courtesy of M. Kaufman, of coherent Ni_3Al precipitates in a Ni matrix. The image was taken near the [001] orientation. The larger cuboidal precipitates grew at the aging temperature of 1100°C while the smaller cube shaped precipitates nucleated during the quenching process.

8.5 nm and large cuboids with an average edge length of approximately 300 nm. The larger cuboids grew during aging while the smaller cubes nucleated during quenching and indicate the existence of precipitate shape transitions. Taking for the material parameters $\sigma = 18.4\ \text{mJ/m}^2$, $\epsilon = 0.0053$ [27] and using the elastic constants cited earlier, a shape transition from cube to cuboid would be expected at about a cube diameter of 125 nm. This critical precipitate size is intermediate between the smaller cubical precipitates and the larger cuboidal precipitates of Fig. 8 and is of the same order as predicted by Khachaturyan [5].

The precipitates of Fig. 8 possess an aspect ratio, $S > 0$ [28] in agreement with the above analysis which predicts that the cube should lose stability with respect to a cuboid possessing aspect ratio $S > 0$ (prolate). However, it should be noted that it is possible with small changes in the elastic constants of the precipitate to change the sign of Φ_3 and, as a result, the direction of the expected precipitate shape transition. The difference in elastic constants between precipitate and matrix may have an important influence on the shape evolution of the precipitate during growth even in the absence of applied stress.

If the presence of an external stress, the bifurcation is broken. The applied stress perturbes the equilibrium shape according to the sign of $-\tau\Delta C_{44}/\epsilon$ for an isotropic system and according to the sign of p or $\tau(\Delta C_{11} - \Delta C_{12})/\epsilon$ for the cubic system with $A > 1$. If these terms are positive, the oblate spheroid is the equilibrium shape at small dimensionless precipitate sizes, otherwise, the prolate spheroid is the equilibrium shape. The stable equilibrium shape at small precipitate sizes remains a stable shape for all precipitate sizes. However, depending upon the magnitude of the applied stress and the difference in elastic constants between precipitate and matrix, there may occur a shift in the global energy minimum from the stable equilibrium shape at small dimensionless sizes to a different shape at large precipitate sizes.

Stress-induced transformations can occur as a result of changes in either the sign or magnitude of p. For small A, however, the transition is discontinuous and may occur with only a change in the magnitude of the external stress. Such a transition indicates the disappearance of the metastable solution.

There exists some disagreement between experimental observations of precipitate shape changes under uniaxial stress that may be partially simplified in terms of the present development. For example, Miyazaki *et al.* [12] observed that Ni_3Al precipitates in a Ni matrix tended to be rod shaped ($S > 0$) with axes aligned in the direction of the external tensile field while Tien and Copley [11] observed plate-

shaped precipitates ($S < 0$) with axes parallel to the tensile field in another Ni–Al-based alloy. It must be noted that these two examples possess large volume fractions, unlike the situation modeled herein. Similar disagreements exist in the Al–Cu system [9, 10] concerning the alignment of θ' plates in an external field.

From the preceeding analysis it is clear that differences in experimental observation may be due to several factors. The most obvious source for potential disagreement centers on those material parameters that influence the sign of the dimensionless stress parameter, p, since changing the sign of p leads to different equilibrium precipitate shapes. For example, in Ni–Al based systems, the sign and magnitude of the precipitate misfit is quite sensitive to the alloy content and to temperature [29]. Small changes in either the chemical composition or aging temperature may result in a change in the sign of the misfit. This would engender a change in sign of the dimensionless stress parameter. The same argument holds true for the difference in elastic constants between precipitate and matrix where small changes in C_{11} or C_{12}, for either phase, may result in the dimensionless stress parameter changing sign. Thus, even the identical alloy system aged under external stress at different temperatures, may exhibit different equilibrium precipitate shapes.

A second possibility for potential disagreement betwen experimental observations under applied stress stems from the existence of metastable precipitate shapes. When the dimensionless precipitate size is greater than one, there may exist more than one precipitate shape that renders the energy of the system a minimum. It is possible for the precipitate to possess a metastable shape due to the specific mechanical (or thermal) history of the alloy. For example, if the alloy is first aged isothermally in the absence of stress, the precipitate may be expected to assume the shape giving the global energy minimum owing to the weak nature of the first order shape transition. If an external stress is then applied, a change in the equilibrium shape results. From the bifurcation diagrams of Figs 3 and 4, one of the new stable equilibrium precipitate shapes will always exist in the vicinity of the equilibrium shape attained by the precipitate in the absence of external stress. However, whether this neighboring equilibrium state is the global equilibrium state or the metastable state in the presence of external stress depends upon the sign of the dimensionless stress parameter, p. The tendency for the precipitate to evolve towards the metastable shape upon application of the external stress is in agreement with a kinetic analysis of the precipitate growth [30]. Once occupying the metastable state, it may be difficult to obtain the global equilibrium state because of a potentially large activation barrier at large dimensionless sizes of the precipitate.

The existence of metastable precipitate shapes may be a source of disagreement between the observations of Miyazaki *et al.* (MNM) and that of Tien and Copley (TC). All specimens of MNM are first preaged for 24 h at 750°C in the absence of external stress. The precipitate shapes after preaging are not cubes, as is usually observed for smaller precipitates, but rods and plates, i.e. shape transitions have occurred owing either to the lose of stability as discussed above, or to precipitate interactions (both MNM and TC have significant volume fractions of the precipitate). Subsequent application of an external tensile stress stabilizes those precipitates aligned in the direction of the external stress and destabilizes the other variants. Therefore, rod shaped precipitates in the direction of the applied tensile stress may be expected. If the Ni–Al system is subjected to the external stress for all aging times, however, an oblate spheroid with axis of revolution parallel to the tensile axis would be expected from the above analysis since $p > 0$ (compare Fig. 3). The oblate spheroid may be either the global energy minimum for all precipitate sizes or, at least, up to some critical size. The jump in the global minimum for this case depends upon the magnitude of the applied tensile field (a sufficiently large applied stress will shift the global minimum from the oblate spheroid to the prolate spheroid). Hence, with the existence of metastable states, the processing history is also important in determining the precipitate shape.

The above analysis and discussion was limited to precipitates whose axis of revolution is constrained to be parallel to the direction of the applied stress. However, MNM show that under a compressive external stress, rod shaped precipitates are observed with the axis of revolution perpendicular to the stress axis. Such shapes and orientations are also permissible stable and metastable precipitate shapes from the symmetry analysis presented here. The existence of these metastable (or, in some cases, stable) states can be inferred from the bifurcation analysis. In the absence of stress, the precipitates align along any of the three [100] variants with equal frequency, the energy of all three states being degenerate. These three variants become apparent if the bifurcation diagrams are drawn with an additional axis depicting the aspect ratio, T. Application of the external stress breaks the symmetry, and the energy of the variant aligned along the direction of the applied stress is different from the two other directions. The bifurcations that existed along the other two variants in the absence of stress are also broken and additional stable equilibrium precipitate shapes become possible. Our analysis shows that these additional states may be either metastable or globally stable depending upon the material parameters and the sign and magnitude of the applied stress. These predictions are in complete agreement with the experimental work of Miyazaki *et al.* [12]. For the Ni–Al case, the two variants with axis of revolution perpendicular to the external stress are the global energy minima.

Tyapkin has examined the effects of stress on low volume fraction Ni–Al and Ni–Cr–Al systems [8]. With the very small misfit exhibited in Ni–Cr–Al, spherical Ni_3Al precipitates become oblate with the axis of revolution in the direction of the uniaxial stress independent of the sign of the stress. The variant morphology in the ternary alloy changes from random to directional alignment. The binary alloy, which possesses a larger misfit, exhibited shape transitions from cubes to plates under tensile load and to rods under compressive loads, the parallelepipeds directed along the stress axis. The variant morphology changes from a cubical array to a directional alignment. Both alloys displayed better alignment along the stress axis than perpendicular to the stress axis for both loading conditions, and curiously better alignment under compression than tensile stress. The symmetries of their observations, both shape and variant morphology, compare directly to our results. The shapes observed also compare to the work of MNM, who examined the binary Ni–Al system.

In the nickel-based alloys, the precipitates are usually found to be ellipsoidal or cuboidal depending upon the magnitude of the precipitate misfit. Precipitates possessing large misfits are cuboidal while those with smaller misfits are spherical. The precipitate may also change shape from sphere to cube during growth. This transition again reflects changes in the relative contributions of the elastic and interfacial energies to the total system energy with increasing precipitate volume. The sphere to cube transition may occur in isotropic as well as anisotropic systems. Although a cube may possess a larger interfacial energy when the interfacial energy is isotropic, its elastic energy may be less. Precipitate volumes at which the sphere to cube transition might occur are easily calculated [7, 23].

In this treatment, the interfacial energy density has been assumed to be independent of crystallographic orientation. This is probably a reasonable assumption for many cubic materials. In many of the nickel-based alloys, spheres are observed for small γ' precipitates, where the interfacial energy is known to dominate the crystal shape. Interfacial energy is no longer dominant near shape transitions, thus any anisotropy plays a smaller role. Also, interfacial anisotropy does not change the qualitative features of the bifurcation analysis because the first term in the Taylor expansion of the interfacial energy is still zero. However, it may change the physical size of the precipitate at which the bifurcation occurs.

Size-induced shape transitions in the absence of an external stress can be modelled as a classical bifurcation problem. The space in which the problem is most efficiently represented is best determined from a symmetry analysis. In this situation, a convenient space is $S - \Lambda$ space. Thus we examine how the equilibrium shape changes as Λ changes and are able to employ all of the well known results of bifurcation theory [24]. A landau-type expansion allows the bifurcation point and the combination of materials parameters that determine the nature of the transition, first-order (transcritical) or second-order (supercritical) to be determined.

The application of an external stress lowers the symmetry of the system and, consequently, breaks the bifurcation observed in the absence of external stress. A convenient approach to determine how the bifurcation is broken and what precipitate shapes would be expected experimentally, is to employ a perturbation analysis [14, 31] assuming that the dimensionless stress parameter is not too large.

Finally, the more formal bifurcation analysis employed here allows the permissible shape transitions to be identified without recourse to numerous system-specific energy calculations. The transitions can be understood in terms of the two dimensionless parameters, Λ and p, rather than the much larger set of materials parameters necessary to conduct the energy calculations (e.g. σ, ϵ, V, τ, and six elastic constants).

5. SUMMARY

Two different types of precipitate shape transitions have been identified, size-induced and stress-induced, that can occur in materials possessing cubic symmetry. The size-induced transition occurs during growth of the precipitate under constant or zero external stress and reflects the changing contributions of the interfacial and elastic energies to the total system energy with precipitate size. A dimensionless precipitate size, Λ, was identified from a bifurcation analysis that succinctly indicates how the various materials parameters interact to stabilize certain precipitate shapes.

Stress-induced transitions occur at constant precipitate size as a result of changing the sign and/or magnitude of the external stress and again reflects changes in the relative contributions of the interfacial and elastic energies to the total system energy with changes in the external stress. From a perturbation analysis, a dimensionless stress parameter was identified, p, that clearly indicates the direction in which an external field breaks the shape bifurcations observed in the absence of an applied stress, and which indicates the nature of the expected transition.

Size-induced shape transitions in the absence of external stress may be first-order, involving a jump to a different precipitate shape or second-order, involving a smooth transition between precipitate shapes with growth of the precipitate. The jump may be from sphere (cube) to either oblate or prolate spheroid (cuboid). The change in precipitate shape occurs in the vicinity of $\Lambda = 1$.

Size-induced transitions in the presence of external stress result only from changes in the global stability of a solution. The stable equilibrium precipitate shape at small sizes remains a linearly stable solution (shape) for all precipitate sizes although other equilibrium shapes can appear at larger precipitate sizes.

Size-induced transitions in the presence of external stress result only from changes in the global stability of a solution. The stable equilibrium precipitate shape at small sizes remain a linearly stable solution (shape) for all precipitate sizes although other equilibrium shapes can appear at larger precipitate sizes.

Stress-induced shape transitions are continuous for precipitates smaller than a critical size (approximately that size corresponding to the bifurcation point in the absence of external stress) and discontinuous for larger sizes. The change in shape on undergoing the transition becomes more pronounced as the magnitude of the external stress increases.

More than one equilibrium precipitate shape may be linearly stable for a given precipitate size and external stress leading to the possibility of the experimentally observed precipitate shape depending upon the thermal or mechanical history of the sample. The observed equilibrium precipitate shape need not be that shape that gives the global energy minimum.

The influence of the external stress on the equilibrium precipitate shape depends on the factor $\Delta C_{11} - \Delta C_{12}$ and *not* on the difference in shear moduli or Young's modulus between precipitate and matrix or on some effective modulus for the system.

Acknowledgements—We are grateful to M. Kaufman for helpful discussions and use of the micrograph, Fig. 8. We also wish to acknowledge the support of the Division of Materials Science of the Department of Energy under grant DE-FG02-84ER45166.

REFERENCES

1. A. J. Ardell, *Phil. Mag.* **16,** 147 (1967).
2. A. J. Ardell and R. B. Nicholson with Appendix by J. D. Eshelby, *Acta metall.* **14,** 1295 (1966).
3. M. Doi, T. Miyazaki and T. Wakatsuki, *Mater. Sci. Engng* **74,** 139 (1985).
4. J. K. Lee, D. M. Barnett and H. I. Aaronson, *Metall. Trans.* **8A,** 963 (1977).
5. A. G. Khachaturyan, *Theory of Structural Transformations in Solids.* Wiley, Berlin (1983).
6. W. C. Johnson and J. W. Cahn, *Acta metall.* **32,** 1925 (1984).
7. A. G. Khachaturyan, S. V. Semenovskaya and J. W. Morris Jr, *Acta metall.* **36,** 1563 (1988).
8. Yu. D. Tyapkin, N. T. Travina, V. P. Kozlov and Y. V. Ugarova, *Fizika Metall. Metalloved.* **42,** 1294 (1976).
9. T. Eto, A Sato and T. Mori, *Acta metall.* **26,** 499 (1978).
10. W. F. Hosford and S. P. Agrawal, *Metall. Trans.* **6A,** 487 (1975).
11. J. K. Tien and S. M. Copley, *Metall. Trans.* **2,** 215 (1971).
12. T. Miyazaki, K. Nakamura and H. Mori, *J. Mater Sci.* **14,** 1827 (1979).
13. A. Pineau, *Acta metall.* **24,** 559 (1976).
14. M. B. Berkenpas, W. C. Johnson and D. E. Laughlin, *J. Mater. Res.* **1,** 635 (1986).
15. W. C. Johnson, D. E. Laughlin and M. B. Berkenpas, Unpublished research.
16. P. Curie, *J. Physique* **3,** (1894).
17. I. S. Zheludev, *Sov. Phys. Cryst.* **2,** 330 (1957).
18. J. W. Cahn and G. Kalonji, *International Conference on Solid-Solid Phase Transformations* (Edited by H. I. Aaronson, D. E. Laughlin, R. F. Sekerka and M. Wayman), p. 3. Metall. Soc. A.I.M.E., Warrendale, Pa (1982).
19. Y. I. Sirotin and M. P. Shaskolskaya, *Fundamentals of Crystal Physics.* Mir, Moscow (1982).
20. M. Doi, T. Miyazaki and T. Wakatsuki, *Mater. Sci. Engng.* **67,** 247 (1984).
21. W. T. Loomis, J. W. Freeman and D. L. Sponseller, *Metall. Trans.* **3,** 989 (1972).
22. W. C. Johnson, *Metall. Trans.* **14A,** 2219 (1983).
23. W. C. Johnson and P. W. Voorhees, *J. appl. Phys.* **61,** 1610 (1987).
24. G. Iooss and D. D. Joseph, *Elementary Stability and Bifurcation Theory.* Springer, Berlin (1980).
25. A. G. Khachaturyan, *Soviet Phys. Solid St.* **9,** 2163 (1967).
26. F. Falk, *J. Physique* **43,** C4-3 (1982).
27. R. G. Faulkner and B. Ralph, *Acta metall.* **20,** 703 (1972).
28. M. J. Kaufman, Private communication.
29. M. V. Nathal, R. A. MacKay and R. G. Garlick, *Mater. Sci. Engng* **75,** 195 (1985).
30. W. C. Johnson, *Metall. Trans.* **18A,** 233 (1987).
31. R. J. Matkowski and E. L. Reiss, *SIAM J. appl. Math.* **33,** 230 (1977).
32. J. D. Eshelby, *Prog. Sol. Mech.* **2,** 89 (1961).

APPENDIX

In this Appendix, a simple Taylor expansion in terms of the aspect ratio S is obtained for the elastic energy of an ellipsoidal precipitate. When the expansion is taken about the sphere, $S = 0$, the following form obtains

$$E^e = \sum_{n=0}^{\infty} \frac{1}{n!} E_n^e S^n \tag{A1}$$

where the Taylor coefficients, E_n^e, are functions of the precipitate volume and the applicable materials parameters. To obtain the Taylor coefficients, we write the elastic energy of an ellipsoidal precipitate embedded in an infinite matrix as

$$E^e = \tfrac{1}{2} V \Delta C_{ijkl} e_{kl}^A (e_{ij}^A + e_{ij}^c) - \tfrac{1}{2} V C_{ijkl}^P (e_{kl}^c - e_{kl}^T) \times e_{ij}^T - V C_{ijkl}^P e_{kl}^T e_{ij}^A \tag{A2}$$

where V is the volume of the precipitate, C is the elastic compliance tensor (a superscript P denoting the precipitate phase), e^T is the transformation strain tensor (assumed constant in V and zero elsewhere), e^A is the strain associated with the applied stress field (assumed uniform within the system) and $\Delta C = C^P - C$. e^c is the constrained strain and is measured with respect to the uniformly stressed matrix phase.

The Taylor coefficients may be obtained numerically for a matrix or cubic anisotropy as the constrained strain may be determined using Eshelby's equivalency relationship [32]. However, the coefficients must be determined for each possible combination of elastic constants. Such system specific calculations do not allow generic relationships between the materials parameters to be obtained that indicate the direction of shape evolution. We therefore obtain the elastic energy to first order in the difference in elastic constants between precipitate and matrix. This approach makes the assumption that

$$|\Delta \bar{C}_{ijkl}| = \left| \frac{\Delta C_{ijkl}}{(C_{11} + 2C_{12})} \right| \ll 1 \tag{A3}$$

where the bar over the elastic constants indicates that each elastic constant has been made dimensionless by the quantity $C_{11} + 2C_{12}$. Higher order contributions of $\Delta \bar{C}$ to the elastic energy are assumed to be negligible.

The constrained strain field may be expressed in terms of an integral equation as [22]

$$e^c_{min}(x) = \frac{1}{2}\int_V [-C^P_{ijkl} e^T_{ij} + \Delta C_{ijkl} e^c_{ij}(\mathbf{x}')] \times [G_{ml,kn}(\mathbf{x}-\mathbf{x}') + G_{nl,km}(\mathbf{x}-\mathbf{x}')]\, dV' \quad (A4)$$

where G is the homogeneous elastic Green's function for an infinite matrix and the comma denotes differentiation with respect to x. It is necessary only to determine the field internal to a precipitate to calculate the Taylor coefficients of equation (1). For an ellipsoid, equation (A4) may be written

$$e^c_{mn}(x) = \bar{C}_{ijkl} e^T_{ij} \bar{S}_{mnkl} + \Delta\bar{C}_{ijkl}[e^T_{ij} - e^c_{ij}]\bar{S}_{mnkl} \quad (A5)$$

where

$$\bar{S}_{mnkl} = \frac{-(C_{11}+2C_{12})}{2}\int_V [G_{ml,kn}(\mathbf{x}-\mathbf{x}') + G_{nl,km}(\mathbf{x}-\mathbf{x}')]\, dV. \quad (A6)$$

If the constrained strain is written to first order in the difference in the elastic constants then

$$e^c_{mn} \approx {}^0e^c_{mn} + {}^1e^c_{mn} \quad (A7)$$

where

$${}^0e^c_{mn} = \bar{C}_{ijkl} e^T_{ij} \bar{S}_{mnkl} \quad (A8)$$

$${}^1e^c_{mn} = \Delta\bar{C}_{ijkl}\bar{S}_{mnkl}[e^T_{ij} - e^A_{ij} - \bar{S}_{ijpq}\bar{C}_{rspq} e^T_{rs}] \quad (A9)$$

${}^1e^c_{mn}$ is the first order correction, due to the different elastic constants, to the constrained strain while ${}^0e^c_{mn}$ is the constrained strain for the elastically homogeneous system. The only shape dependent terms are contained with the tensor $\bar{S}$ which can be written as

$$\bar{S}_{mnkl} = \frac{(C_{11}+2C_{12})}{8\pi}\int_\Omega Q(a_1,a_2,a_3) \times [z_n z_l M^{-1}_{mk} + z_m z_l M^{-1}_{nk}]d\Omega \quad (A10)$$

$$Q(a_1,a_2,a_3) = a_1 a_2 a_3 [a_1^2 z_1^2 + a_2^2 z_2^2 + a_3^2 z_3^2]^{-3/2} \quad (A11)$$

$$M_{jm} = z_i z_k C_{ijkm} \quad (A12)$$

where the integration is performed over a unit sphere, the a_i are the axes of the ellipsoid and z is a unit vector.

We now assume cubic anisotropy for both precipitate and matrix phases, the transformation strain is dilatational and of the form $e^T_{ij} = \epsilon\delta_{ij}$, the axes of the ellipsoid coincide with the cube axes of both phases and the applied stress, σ^A, is uniaxial and directed along the x_3 axis. Substituting the expressions for the constrained strain into Eq. (A-2) for the elastic energy, allows determination of the Taylor coefficients as

$$E^c_0 = L^*_0 + K^*_0 + \frac{V(C_{11}+2C_{12})}{2}\left\{3\epsilon^2(\bar{C}^P_{11}+2\bar{C}^P_{12}) - \frac{2\epsilon\tau(\bar{C}_{11}-\bar{C}_{12})(\bar{C}^P_{11}+2\bar{C}^P_{12})}{(\bar{C}_{11}+\bar{C}_{12})} + \Delta\bar{C}_{ijkl}e^A_{ij}e^A_{kl}\right\} \quad (A13)$$

$$E^c_n = L^*_n + K^*_n (n \geqslant 1) \quad (A14)$$

$$L^*_n = \frac{V\epsilon^2(C_{11}+2C_{12})}{2}L_n \quad (A15)$$

$$K^*_n = \frac{V\epsilon\tau(C_{11}+2C_{12})^2}{(C_{11}+C_{12})}K_n \quad (A16)$$

$$L_n = -F_n[1+2(\Delta\bar{C}_{11}+2\Delta\bar{C}_{12})] + \Delta\bar{C}_{12}G_n + (\Delta\bar{C}_{11}-\Delta\bar{C}_{12})H_n \quad (A17)$$

$$K_n = (\bar{C}_{11}\Delta\bar{C}_{12} - \bar{C}_{12}\Delta\bar{C}_{11})F_n + (\Delta\bar{C}_{11}-\Delta\bar{C}_{12})I_n \quad (A18)$$

$$F = \bar{S}_{nnkk} \quad (A19)$$

$$G = (\bar{S}_{nnkk})^2 \quad (A20)$$

$$H = \bar{S}_{nnkk}\bar{S}_{kkpp} \quad (A21)$$

$$I = \bar{S}_{pp33} \quad (A22)$$

$$F_i = \left(\frac{\partial^i F}{\partial S^i}\right)_{S=0} \quad (A23)$$

$$\tau = \frac{\sigma^A(C_{11}+C_{12})}{(C_{11}-C_{12})(C_{11}+2C_{12})}. \quad (A24)$$

The Taylor coefficients to the elastic energy require solving several surface integrals which depend only upon the elastic constants of the matrix phase.